Dalton Transactions

The effect of outer-sphere anions on the spectroscopic response of metal-binding chemosensors

Journal:	*Dalton Transactions*
Manuscript ID	DT-COM-06-2022-001794.R1
Article Type:	Paper
Date Submitted by the Author:	27-Jul-2022
Complete List of Authors:	Ihde, Michael; The University of Alabama, Department of Chemistry and Biochemistry; Hamilton College, Covey, Gabrielle; The University of Alabama, Department of Chemistry and Biochemistry Johnson, Ashley; University of Southern Mississippi, Department of Chemistry and Biochemistry Fronczek, Frank; Louisiana State University, Department of Chemistry Wallace, Karl; University of Southern Mississippi, Department of Chemistry and Biochemistry Bonizzoni, Marco; The University of Alabama, Department of Chemistry and Biochemistry; The University of Alabama, Alabama Water Institute

ARTICLE

The effect of outer-sphere anions on the spectroscopic response of metal-binding chemosensors

Received 00th January 20xx,
Accepted 00th January 20xx

DOI: 10.1039/x0xx00000x

Michael H. Ihde,[a] Gabrielle Covey,[a] Ashley D. G. Johnson,[b] Frank R. Fronczek,[c] Karl J. Wallace,[b] and Marco Bonizzoni*[a,d]

Ion pair receptors typically contain two separate binding sites, for the metal and the anion respectively. Here we report a less synthetically demanding approach, whereby we prepared a family of ion pair sensors based on a rhodamine fluorescent scaffold containing a tunable cation binding motif. When exposed to ion pairs, a competition for the metal ion is established between these ligands and anions. Structural and spectroscopic evidence showed that anions bind through weaker secondary interactions in the metal's outer coordination sphere and their presence influences the optical spectroscopic properties of the coordination complex in distinctive ways. The relationship between the binding site's metal affinity and its tunable properties, and the sensors' discriminatory power for anions was explained as a function of the metal ion's binding preferences. These effects were also exploited to discriminate cations and anions concurrently through multivariate data analysis methods.

Introduction

Ditopic ion pair receptors have shown good binding affinities,[1] and opportunity for ion pair extraction and transport applications.[2, 3] Such receptors contain two separate binding sites, i.e., one site for the anion and a second for the cation.[4-6] One of the earliest ditopic receptors was reported in 1991 by Reetz et al., who used a crown ether moiety for K^+ cation binding coupled with a Lewis acidic boron unit for anion coordination (e.g. F^-, CN^-).[7] This has led to more recent examples by Sessler et al., including functionalized calix[4]pyrrole and calix[4]arene derivatives combined with a crown ether moiety for dual alkali metal cation and anion binding (e.g., CsCl, CsF, $CsNO_3$).[8, 9] Light-emitting ion pair receptors have been widely used for analytical detection, with the first fluorogenic ion pair sensor reported by de Silva and coworkers in 1996 for biologically relevant amino acid zwitterions.[10] Since then, numerous fluorometric ion pair sensors have been developed for biologically and environmentally relevant ion pairs and zwitterions.[11-14]

Although some ion pair receptors have been adapted to work in aqueous media, there are many important industrial applications that function in non-aqueous solvents. For instance, non-aqueous systems have been used to facilitate the solubilisation of inorganic salts in organic media,[15-18] e.g., as phase-transfer agents in catalysis.[19, 20] Ion pair receptors also work as efficient extraction and membrane transport agents,[21-23] and are used in industrial purification processes based on liquid membrane transport.[24, 25] Extraction of radioactive materials from saline solutions for safe disposal, as is the case for spent pertechnetate and perrhenate salts used in nuclear medicine, also relies on non-aqueous ion pair recognition.[26] It is therefore of great interest to develop ion pair receptors and sensors adapted to non-aqueous organic media.

To achieve strong and selective binding, these receptors often require complex synthesis; they may also suffer from a restricted scope, targeting *s*-block metal cations or more charge-diffuse organic cations (e.g., ammonium cations). Single-site monotopic systems would alleviate the design and synthesis burden associated with ditopic receptors, i.e., the *ad hoc* synthesis of two or more receptor counterparts on a single molecule for a specific ion pair. Monotopic receptors achieve ion pair sensing by taking advantage of differential binding caused by counterion effects, i.e., the influence of cation-anion and counterion-solvent interactions on the binding affinity of the target analyte to a given receptor.[27-29]

Most efforts in this field, however, have focused on ditopic receptors, targeting only one or two ion pairs, with each sensor designed with two independent binding sites that are specifically constructed to bind strongly and selectively to the analytes of interest. We show here that a broader response can be achieved using a monotopic sensor, retaining good selectivity and alleviating the synthesis requirements. Conversely, in this approach we demonstrate that the most effective sensor was the one that displayed intermediate binding affinity with heavy metal cations, thus allowing anions to effectively compete for the metal ion.

[a] Department of Chemistry and Biochemistry, The University of Alabama, Tuscaloosa, AL 35487-0336, United States.
[b] Department of Chemistry and Biochemistry, The University of Southern Mississippi, Hattiesburg, MS 39406, United States.
[c] Department of Chemistry, Louisiana State University, Baton Rouge, LA 70803, United States
[d] Alabama Water Institute, The University of Alabama, Tuscaloosa, AL 35487-0206, United States.

Electronic Supplementary Information (ESI) available: further XRD details and crystal structure data; representative metal titration spectra and binding constant determination details. See DOI: 10.1039/x0xx00000x

For this study three monotopic rhodamine-based receptors have been prepared. They all contain a single metal binding domain including a secondary motif that changes the domain's overall binding nature and strength. Moreover, the binding response is modulated by the nature of the accompanying counter-anions. We discuss the effects of the counterion and the balance between the metal binding affinity of the sensors and the ion pairing tendencies of the counterion, and we further show how these properties can be exploited to provide discrimination of heavy metal ion pairs. The system described here offers a desirable turn-on fluorescence response capable of discriminating among ion pairs, using only one chelating motif, with different binding domains.

Rhodamine-based fluorescent derivatives have been developed with a wide range of substituents and with emission spanning the visible and infrared spectrum,[30] high quantum yields (>90%), and good photostability have made this class of molecules attractive for many applications, including fluorescence, biological imaging and labelling, fluorescence signal standardization, molecular switches, and chemosensors for a variety of analytes.[31] In fact, rhodamine derivatives possessing a non-fluorescent spirolactam form display a dramatic turn-on fluorescence response upon ring opening, which can be triggered by e.g. metal ion binding to construct chemosensing systems.[32-34]

In this work, three rhodamine 6G derivatives containing distinct metal binding moieties are reported. Covalently attached to the dyes is an amide group, an imine moiety, and differing aryl units (see Figure 1): benzene (**Rh-benz**), phenol (**Rh-phen**), and pyridine (**Rh-pyr**). These pendant arms were chosen to provide a range of binding affinities and metal binding modes (e.g., chelate ring size, and the availability of hard/soft binding sites), allowing us to systematically investigate these factors on the overall binding behaviour of these chemosensors.

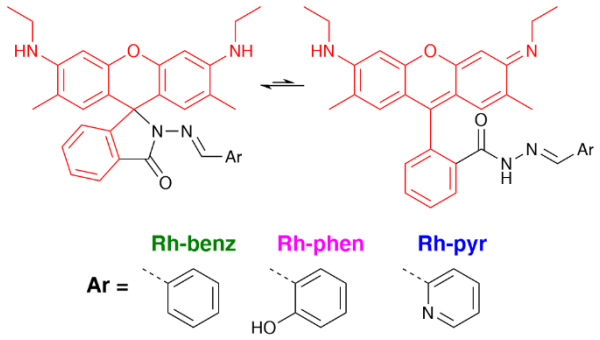

Figure 1. Chemical structures of the **Rh** rhodamine 6G derivatives used as monotopic ion pair sensors. The red structure indicates the rhodamine 6G core; the metal binding groups are highlighted in black. The ring-closed form (spirolactam, left) and open form (right) of these sensors are both shown.

Results and Discussion

Synthesis of chemosensors

The three molecular sensors **Rh-benz**, **Rh-phen**, and **Rh-pyr** were prepared in a two-step procedure whereby commercially available rhodamine 6G chloride was reacted with excess hydrazine hydrate and the hydrazide was isolated as a pink solid. Further functionalization was carried out by condensation of the free amine in the hydrazide with an appropriate aldehyde derivative to form an imine in methanol. The resulting **Rh** molecular sensors were obtained in excellent yields (80-90%) and were fully characterized (see Scheme 1).

X-ray crystal structure of Rh-benz

A single crystal of **Rh-benz** was grown by slow evaporation of a saturated solution in methanol over several days. The compound crystallized in the triclinic crystal system in the $P\bar{1}$ space group, with an asymmetric unit cell made up of two independent molecules forming a dimer (Figure 2). Two dimers are related in a centrosymmetric fashion in the unit cell (Z = 4). Both molecules show the typical cyclic (sp^3) spiro-ring system, wherein the benzoheterocycle ends up orthogonal to the xanthene moiety. This geometry is stabilized by an intramolecular CH···π interaction (Figure 2b). Interestingly, one of the xanthene groups in the dimer is planar (Figure 2a and 2c, molecule (1)), whereas the other xanthene in the dimer has subtle curvature (Figure 2a and 2c, molecule (2)). The C=N (C21-N2) bond lengths in the hydrazone group are 1.282(3) Å and 1.281(2) Å for molecules 1 and 2, respectively; the C21-N2-N1 and C54-N5-N6 bond angles are 120.39(16)° and 119.38(16)°, respectively, i.e., an ideal sp^2 hybridized nitrogen atom. The C21=N2 double bond of the hydrazone is found in the *trans* configuration. Moreover, the molecule's three aromatic ring systems lie in different planes (Figure 2d), identified as the

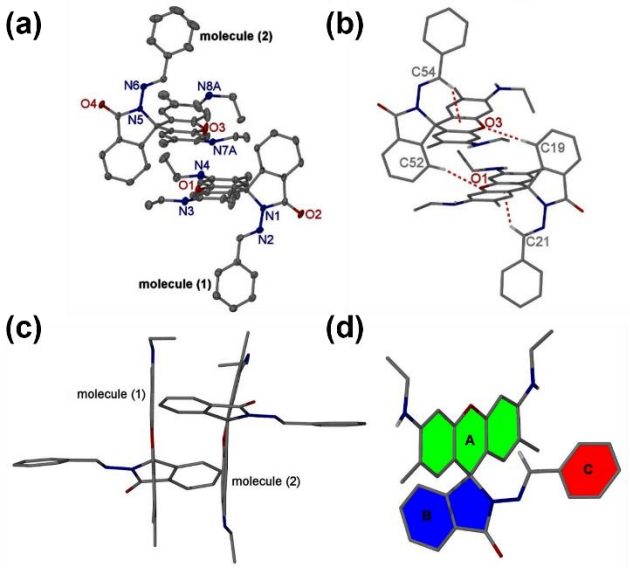

Figure 2. Structures from single-crystal diffraction experiments for **Rh-benz**. **(a)** View of two molecules forming a dimer (displacement ellipsoids shown at 50% probability). **(b)** the intra- and intermolecular hydrogen bonding interactions stabilizing the dimer; C21···π = 2.37 Å; C54···π = 2.39 Å; the (D···A) distance C19···O3 = 3.304(2) Å; and C52···O1 = 3.357(2) Å. **(c)** A side-on view of the two molecular partners forming a dimer in the crystal structure of the **Rh Benz** ligand. The aromatic xanthene group of molecule (1) is planar, whereas the same moiety in molecule (2) shows some curvature. **(d)** The three different planes evident in molecule (1).

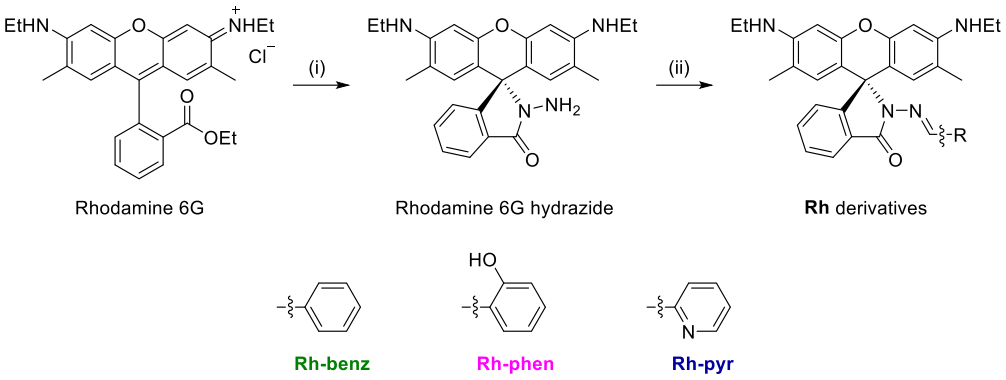

Scheme 1. Synthesis of sensors **Rh-benz**, **Rh-phen**, **Rh-pyr**: (i) hydrazine hydrate in MeOH, Δ 4 hr (ii) aromatic aldehyde in MeOH, Δ 6 hr. Typical yields 80 to 90% (aromatic aldehydes: benzaldehyde, 2-hydroxybenzaldehyde, and pyridine-2-carbaldehyde).

xanthene (plane A), benzoheterocycle (plane B), and the benzene ring (plane C). The dimer is also stabilized by a hydrogen bonding interaction between the O1 oxygen of the xanthene group and C(52)-H of the adjacent molecule, and by an intramolecular CH···π interaction shown in Figure 2b. No π-π stacking interactions could be identified in the crystal packing, even though the structure is rich in aromatic moieties. Interestingly, the crystal packing has an array of hydrogen bonding motifs, ranging in strength from weak to medium, and comprising of CH to oxygen or CH to nitrogen interactions (ESI Figure S1). Only one of the NH functional groups (EtNH) seems to participate in hydrogen bonding, through an NH···π(C=N) interaction.

Optical spectroscopic data

Optical spectroscopic measurements were carried out in acetonitrile solution, to mimic the non-aqueous media of potential application for these systems. The molecular sensors **Rh-benz**, **Rh-phen**, and **Rh-pyr** displayed a pronounced turn-on fluorescence response upon addition of three *d*-block metal cations (Cu(II), Zn(II), and Fe(III)). In this study, Cu(II) and Zn(II) were chosen as representative open- and closed-shell metal ions, whereas Fe(III) was included for its much higher Lewis acidity compared to Cu(II) and Zn(II). For each cation, triflate, chloride, and acetate counterions were used. These anions, which exhibit distinctly different coordinative strength (weak, medium, and strongly coordinating respectively), were selected to investigate the anion's effect on metal binding in acetonitrile solution, where ion pairing is expected to be pronounced.[35, 36] In the context of ion pairing, the three anions were chosen as representative examples across the Hofmeister series. As a result, we might expect that another medium-binding counterion such as bromide, chloride's neighbour in the Hofmeister series, would exert similar effects on solvent structure and through Lewis basicity.[37, 38] Similar considerations also apply to the triflate anion, included here as a representative of e.g. trifluoroborate and other poorly binding counterions.

Ion pairing interactions were detectable through their effect on the spectroscopic signal of these metal complexes. Since iron(III) acetate (also referred to as basic iron acetate) is a trinuclear species with intricate reactivity of its own, we chose to forgo its use in favour of iron(III) acetylacetonate ($Fe(acac)_3$), which provided a closer comparison to other metal acetates in this series. Therefore, the following nine ion pairs were considered in this study: $Cu(OTf)_2$, $CuCl_2$, $Cu(OAc)_2$, $Zn(OTf)_2$, $ZnCl_2$, $Zn(OAc)_2$, $Fe(OTf)_3$, $FeCl_3$, and $Fe(acac)_3$.

The metal binding properties of these chemosensors were initially studied using $Zn(OTf)_2$ as a binding probe. The Zn(II) ion, (d^{10}) was expected to provide the least complicated binding behaviour; similarly, triflate was used as a weakly binding counterion among those under study. In acetonitrile solution the three **Rh** sensors were found in the colourless and non-fluorescent spirolactam form. Upon addition of $Zn(OTf)_2$ to any of the three sensors, the solution assumed the typical pink hue of rhodamine 6G and a corresponding turn-on fluorescence response was observed (see Figure 3a), indicating that the metal ions were able to trigger the conversion of the spiro form to the spectroscopically active ring-opened form.

Upon excitation between 310-450 nm, a dramatic increase in fluorescence intensity was measured, with an emission maximum at ca. 554 nm (Figure 3b-d). The excitation wavelength for each dye was chosen to correspond to an area in the absorbance titration spectra with either an isosbestic point or where no new absorbance peaks emerged, so changes in the fluorescence emission could be safely ascribed to

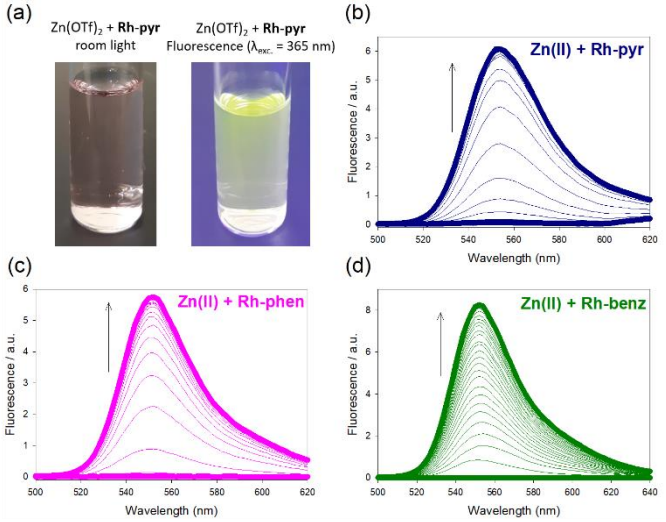

Figure 3. (a) Image of the **Rh-pyr** probe with $Zn(OTf)_2$ displaying the distinct pink colour of the rhodamine backbone, and its fluorescence emission under UV irradiation. (b-d) Steady-state fluorescence spectra of (b) **Rh-pyr** (λ_{exc} = 314 nm), (c) **Rh-phen** (λ_{exc} = 350 nm), and (d) **Rh-benz** (λ_{exc} = 450 nm), upon the addition of $Zn(OTf)_2$. All titrations were carried out in acetonitrile ([**Rh**] = 2.5 μM and [metal] = 0-23.3 μM).

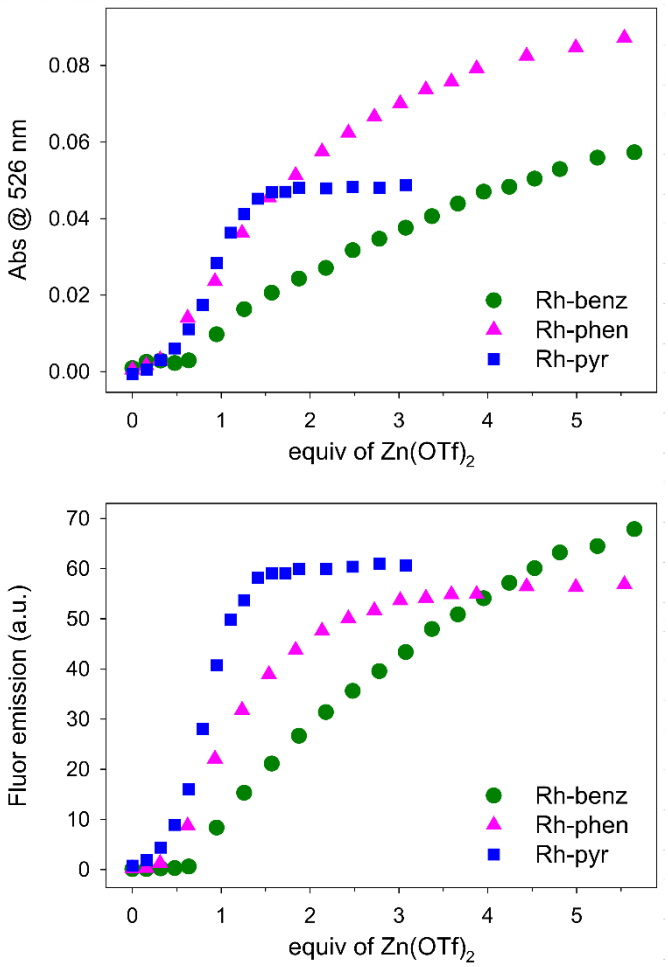

Figure 4. Comparison between absorbance (top) and fluorescence emission (bottom) binding isotherms for **Rh-benz, Rh-phen**, **Rh-pyr** upon addition of $Zn(OTf)_2$. Emission wavelength: 526 nm; excitation for **Rh-pyr** = 314 nm, **Rh-phen** = 350 nm, and **Rh-benz** = 450 nm. All measurements in acetonitrile ([sensor] = 2.5 μM, [metal] = 0-23.3 μM).

chemical interactions, and not to adventitious changes in excitation efficiency. For example, we avoided excitation at the traditional rhodamine absorbance peak at ca. 522 nm, where absorbance increased upon the addition of metal ions.

In the case of Zn(II), the fluorescence emission reached a plateau after adding excess Zn(II) ions. Conversely, paramagnetic transition metal ions with a partially filled *d*-shell (Cu(II) and Fe(III)) caused some degree of emission quenching, likely through photoinduced electron transfer (PET); this is apparent in the interaction of **Rh-pyr** with $Cu(OTf)_2$, whose emission in the presence of $Cu(OTf)_2$ was four times lower than that obtained from the same dye with $Zn(OTf)_2$. A complete set of absorbance and fluorescence titrations for all dyes with each metal triflate salt is presented in the Supporting Information (Figure S2 and S3). A set of titration isotherms is also provided in Figure 4 to compare the different binding affinities and complex stoichiometries exhibited by the three **Rh** sensors when exposed to $Zn(OTf)_2$, as a representative example.

Binding constant determination

Binding constants were obtained from the absorbance data by nonlinear model fitting (see Table 1 and Figures S4-S9 for details on the binding models and fitting results).[39] In general, strong binding was observed for the 1:1 complex formation for all three sensors (log K_{11} > 5, see Table 1), with increasing binding affinity in the order of **Rh-benz** < **Rh-pyr** < **Rh-phen**. This trend is likely due to the binding tendencies of the plain benzene vs. pyridine vs. phenol/phenolate pendant rings: in fact, these arms contain no additional metal binding site (**Rh-benz**) vs. one additional weak binding site (**Rh-pyr**) vs. one additional strong binding site (**Rh-phen**), respectively (Figure 5).

Table 1 Formation constants for representative results obtained from the complexation of Zn(II) triflate to the three sensors. The concentration of the sensor molecule was maintained constant at 2.5×10^{-6} M. Experiments were run in acetonitrile at 25 °C.

		log K_{11}	log K_{21}	log β
Rh-benz	$Zn(OTf)_2$	5.63(4)	5.3(2)	11.0(3)
Rh-pyr	$Zn(OTf)_2$	6.81(9)	–	–
Rh-phen	$Zn(OTf)_2$	7.57(2)	6.15(8) 5.42(2)[a]	13.72(7) 13.00(2)[a]

K_{21} refers to the formation constant for the species containing two probe molecules per metal ion. In cases indicated with (a), a species containing 2 metal ions per sensor was observed; this corresponds to a K_{12} formation constant.

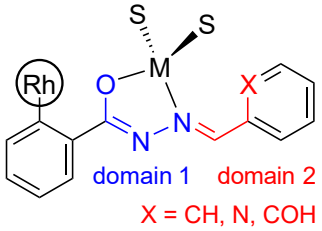

Figure 5. Chelating motifs in the pendant arm of the **Rh** sensors. **Rh-benz** provides no secondary binding interaction; **Rh-pyr** and **Rh-phen** provide a pyridine and a phenol binding site, respectively. In this structure, Rh represents the xanthene moiety common to all three sensors.

Comparing titrations obtained for each **Rh** sensor upon the addition of three metal triflate salts, we noticed clear differential response patterns associated with the nature of the metal ion (see Figure 4). In other words, associated ion pairs behaved as distinct chemical species because the anions modulated the binding behaviour and affinity of the accompanying metal cation. The process can be envisioned as a competition between the receptors and the anions to form a complex with the metal ion. We demonstrate here that this phenomenon, often overlooked or purposefully minimized in traditional ion receptors, can be harnessed to provide analytically useful differential responses to transition metal ions and their counterions: although the anions do not bind directly to our receptors, the metals' binding is influenced by the presence and nature of the anions, so ion pairs display nuanced binding behaviour with these receptors and can be detected as separate species.

Despite the abundance of X-ray crystal structures for rhodamine and its derivatives, there are only a handful of solid-state structures in which rhodamine derivatives act as a ligand to coordinate with metal centres. These can help us understand the coordination environment of the metal centre and give us

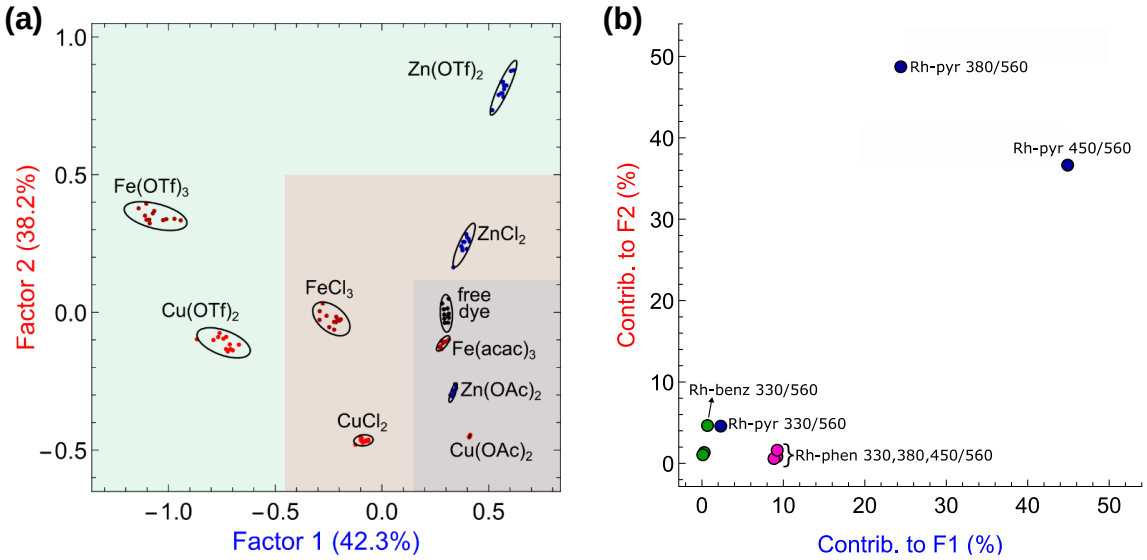

Figure 6. (a) Two-dimensional LDA scores plot for the differentiation of nine ion pairs containing *d*-block metal ions, using nine fluorescence measurements from three rhodamine-based single-site fluorescent sensors. After reduction to two dimensions, the plot captures 80.5% of the total information content from the original data set. [**Rh** sensor] = 2.5 μM and [analytes] = 25 μM in acetonitrile. **(b)** Corresponding loadings plot for the ion pairs data set, indicating the relative contributions of each instrumental measurement to the first two LDA factors. Blue circles: contributions from fluorescence measurements of the **Rh-pyr** dye; pink circles: the **Rh-phen** dye; green circles: the **Rh-benz**

insight into the structural role of the counter anion. Rhodamine complexes have been reported for Ag(I) and Hg(II),[40] Cd(II),[41] Cu(II),[42] Pd(II),[43] Zn(II),[44] as either discrete coordination complexes or clusters.[40] For metals that favour coordination number four, tetrahedral and square planar geometries are the most common: in these the rhodamine derivative will coordinate in mono, di, and tridentate fashion in the different domains (Figure 5). The remaining positions in the coordination sphere are occupied either by a solvent molecule or by a counter-anion, often a chloride or acetate. A great diversity of coordination arrangements was observed when rhodamines act as ligands, even in the small number of such solid-state structures reported so far. This mirrors the multiple species postulated in solution to model our binding isotherms, as detailed in Table 1 and in the binding constant determination section of the Supporting Information. In agreement with the solid-state structures, dimers and clusters are likely to exist in solution as well, together with multinuclear species with anions acting as a bridge between metal centres.

Multivariate analysis

To support this hypothesis, we repeated the titration experiments described above with all combinations of three metal ions (Cu(II), Zn(II), and Fe(III)), and three counter-anions (triflate, chloride, and acetate/acac) with very different binding preferences.[45] We switched to using a microwell plate reader and 384-well microplates for rapid data acquisition on multiple samples, with 12 replicates per sample. Solutions containing one of the three **Rh** sensors and one of the nine ion pairs were arranged on a 384-well microplate ([sensor] = 2.5 μM, [metal] = 25 μM) and fluorescence measurements were collected using bandpass filters to select appropriate excitation and emission spectral windows (namely, $\lambda_{exc}/\lambda_{em}$: 330/560 nm, 380/560 nm, and 450/560 nm).

Using linear discriminant analysis (LDA) we generated new descriptor variables (*factors*) as linear combinations of the original fluorescence measurements to maximize separation between different ion pairs.[46, 47] A visual representation of these results was obtained by using each ion pair's factor scores as coordinates in 2D scatter plots known as *scores plots*. The resulting 2D scores plot, presented in Figure 6a, indicates that all nine ion pairs showed differential binding behaviour due to counterion effects, with excellent separation among them. Replicates for each sample (i.e., individual points in the scores plot) were clustered tightly together, indicating excellent reproducibility. Furthermore, clear "supercluster" groupings of anions and metal cations emerged from these results in characteristic positions in the 2D factor space, highlighted as regions of distinct colour in Figure 6a. For instance, acetate and chloride anions fell closest to the "free dye" reference cluster, whereas the triflate salts were much farther away from it. We interpret this as stemming from the different degrees of association in ion pairs formed by acetate (most tightly bound) vs. chloride (medium binding) vs. triflate (loosely associated in solution). This is consistent with the overall binding model proposed above, which postulates that the strength of these secondary interactions is driven by a competition for the metal ion between the **Rh** sensors and the counter-anions. In this context, the stronger-binding acetate competes very effectively for the metal ion, resulting in comparatively weaker interactions between the metals and the **Rh** sensors, and therefore poorer differentiation among metal ions. On the other hand, higher dissociation of the triflate salts in acetonitrile solution allowed for stronger interactions between the metal ions and the **Rh** sensors, providing a broader dynamic range in the instrumental responses and, therefore, more effective differentiation.

Analysis of the corresponding factor loadings, i.e., the contributions of each instrumental measurement to the LDA factors (Figure 6b) supports this hypothesis as well. In fact, the rhodamine-pyridine (**Rh-pyr**) derivative was found to be the

overall most important contributor to the differentiation, whereas the **Rh-phen** and **Rh-benz** probes contributed much less (<10% to the first two factors). The relative values of the Zn(II) triflate binding constants (Table 1) with our three ligands indicate that **Rh-pyr** behaves as an intermediate-strength ligand thanks to its pyridine secondary binding site (Figure 5). In fact, as mentioned above in the binding constant discussion, its affinity is intermediate between the weaker-binding **Rh-benz** (no secondary binding site), and the stronger binding **Rh-phen** (phenol binding site). Since we propose that counterion differentiation depends on the establishment of an effective competition for the metal ion between the **Rh** ligand and the anions, then **Rh-benz** unfortunately poses no competition to the anion, so anions all behave similarly, and their ion pairs are poorly differentiated. On the opposite end of the scale, **Rh-phen** presents *too strong* a competition to the anions, so no anion can successfully compete with it for the metal, and the anions' behaviour in its presence is equally undifferentiated. Only **Rh-pyr**'s intermediate binding affinity provides an appropriate degree of competition to anions, highlighting their intrinsic differences to be harnessed for the differentiation of their ion pairs.

Conclusions

In summary, three rhodamine derivatives containing metal binding sites of varying strength were synthesized and their binding behaviour towards transition metal ions and their anionic counterions was explained in light of the anions' intrinsic metal binding properties and of the sensors' structure. In these systems, metal binding converts the non-fluorescent spirolactam to a fluorescent open form in acetonitrile solution, producing a strong and variable turn-on fluorescence signal in the presence of different metal salts. These sensors were also shown to have applications as effective turn-on fluorescent sensors for transition metal cations *and* their anionic counterions. Since the latter significantly influence the metal binding in these systems, the differential binding interactions of the metal cations to the **Rh** sensors could be harnessed for the identification of both metal cations *and* their counterions using only single-site metal-binding receptors, eschewing the need for specialized cation and anion binding sites in the same receptors.

Experimental Section

Materials and methods

Rhodamine 6G hydrochloride, hydrazine hydrate, 2-hydroxybenzaldehyde, and pyridine-2-carbaldehyde were purchased from Millipore Sigma and used without further purification. Reaction solvents (methanol and diethyl ether) were obtained from Fisher Scientific, and deuterated solvents from Cambridge Isotopes. All spectroscopy experiments were performed in spectroscopic-grade acetonitrile (from Alfa Aesar), unless otherwise stated. For consistency, stock solutions for all dyes and metal salts were prepared fresh before each experiment. Stock solutions of rhodamine dye derivatives were prepared by adding appropriate amount of solid ligand to volumetric flasks and filling to volume. All metal salt stock solutions were prepared by adding an appropriate amount of solid salt (Fluka) to 10 mL of acetonitrile. Any hygroscopic salts (metal triflate salts and zinc(II) chloride) were stored in a desiccator before use.

Instrumentation

^{1}H-NMR spectra were acquired on a Bruker Avance 400 operating at a proton frequency of 400.13 MHz, equipped with a standard BFO 5 mm two-channel probe, in the appropriate deuterated solvents. Chemical shifts are reported in parts per million (ppm) downfield from tetramethylsilane (0 ppm) as the internal standard and coupling constants (*J*) are recorded in hertz (Hz). All spectra were recorded at ambient temperature. Low resolution mass spectra were measured with a Finnigan TSQ70 triple quadrupole instrument. IR spectra were obtained on a Nicolet Summit FT-IR spectrometer paired with a Smart Orbit attenuated total reflection (ATR) attachment. The characteristic peaks are reported in wavenumbers (cm^{-1}) and are described as weak (w), medium (m), strong (s), and very strong (vs). Elemental analysis was carried out by Atlantic Microlab, GA. X-ray single crystal data collection and analysis were carried out at Louisiana State University using a Bruker APEX2. UV-vis absorbance measurements were performed on a Hewlett-Packard 8452a diode array spectrophotometer. Steady-state fluorescence measurements were performed with an ISS PC1 spectrofluorometer. Excitation was carried out using a broad-spectrum high pressure xenon lamp (CERMAX 300W). Excitation correction was performed through a rhodamine B quantum counter with a dedicated detector. Excitation intensity was controlled by a manually operated iris, which was kept fully open for all titrations. Spectral resolution was controlled by manually operated calibrated slits. Detection occurred through a Hamamatsu red-sensitive PMT. For all absorbance and fluorescence measurements, the temperature (25 °C) was controlled by an external circulating water bath. Multivariate spectroscopic data was acquired on a BioTek *Synergy II* multimode microwell plate reader, capable of measuring steady-state fluorescence spectra through a set of bandpass filters. The sample compartment in this instrument is electrically thermostatted to 25 °C.

X-ray structure determination

Cell refinement and data reduction were carried out using Bruker SAINT; the structure was solved using SHELX97,[48, 49] and refined using SHELXL2013.[48] Graphics were generated using X-Seed.[50] Crystallographic tables for **Rh-Benz** are shown in the Supporting Information. The crystal structure of **Rh-Benz** has been deposited into the CCDC (2168004).

Metal binding titrations

To assess the binding properties of metal ions to these rhodamine-based sensors, absorbance and fluorescence spectra were collected upon addition of aliquots of a titrant solution that contained metal triflate and one of the **Rh** sensors, into a solution containing an equal concentration of **Rh** sensors

in acetonitrile. These experiments were carried out with all three rhodamine 6G fluorescent probes **Rh-benz**, **Rh-phen**, and **Rh-pyr**. The resulting absorbance spectra are presented in Figure S2. Shown in Figure S3 are the fluorescence titration spectra of the three rhodamine-based **Rh** probes upon the addition of $Cu(OTf)_2$ and $Fe(OTf)_3$.

An aliquot of dye stock solution was added to a 1 cm quartz cell to prepare a 2.5 μM solution of dye. Aliquots of each metal triflate stock solution (5-20 μL) was added to the cuvette before each measurement. Metal concentrations in the cuvette ranged from 0-25 μM.

Binding constant determination

Binding constants were obtained through non-linear fitting of the absorbance and fluorescence titration data to a sequential binding model involving multiple formed species. The analysis and fitting were carried out using *HypSpec*.[51] Details on the binding models used, and comparisons of the fitting results with experimental data, are shown in the Supporting Information.

Multivariate experiments

Experiments were laid out by hand using Eppendorf Research multichannel pipettors and disposable plastic tips into Aurora 384-well configuration non-treated cyclo-olefin polymer (COP) black microwell plates with clear bottom for fluorescence spectroscopy. Each fluorescent probe was laid out and then nine freshly prepared metal salt stock solutions ($Zn(OTf)_2$, $ZnCl_2$, $Zn(OAc)_2$, $Cu(OTf)_2$, $CuCl_2$, $Cu(OAc)_2$, $Fe(OTf)_3$, $FeCl_3$, and $Fe(acac)_3$) were added to give 12 replicates of metal salt-dye. The total volume for each well was 100 μL. Additionally, eight replicates of acetonitrile solvent (for blanking), and eight replicates of each fluorescent probe (as a reference) were added to the plate. Dye concentrations were 2.5 μM and salt concentrations were 25 μM. Multivariate analysis was based on three instrumental measurements for each rhodamine probe (nine total per sample). Fluorescence measurements were collected using three bandpass filters for excitation (λ_{exc} = 330±10 nm, 380±10 nm, 450±25 nm), and the same bandpass filter for emission (λ_{em} = 560±20 nm). Plates were measured immediately after preparation. Reading time for the entire plate required about 10-15 minutes. There appeared to be no evaporation of the acetonitrile solvent in this time span, and therefore the plate did not need to be sealed.

Linear discriminant analysis (LDA)

To evaluate the discriminatory power of the molecular probes, Linear Discriminant Analysis (LDA) was used to interpret the resultant data set. All multivariate analyses were performed in the commercial *Mathematica* program (release 12.3.1) published by Wolfram Research Inc., using routines developed in-house.

Preparation of rhodamine 6G hydrazide

Rhodamine 6G (1.0 g, 2.1 mmol) was dissolved in methanol (25 mL). Hydrazine hydrate (1.53 g, 30 mmol) in methanol (10 mL) was added dropwise to the rhodamine 6G solution over ten minutes with continuous stirring. The solution was allowed to reflux for 4 hours, during which time a pink precipitate formed. The precipitate was filtered and washed with cold water (3 × 100 mL) and dried in a desiccator. Yield 0.86 g (2.0 mmol, 96%). ^{1}H NMR (400 MHz, $CDCl_3$) δ (ppm): 7.98 - 7.95 (1H, m), 7.46 (2H, td, *J* = 2.4, 3.9 Hz), 7.08 - 7.05 (1H, m), 6.39 (2H, s), 6.26 (2H, d, *J* = 0.5 Hz), 3.58 (2H, s), 3.52 (2H, t, *J* = 4.5 Hz), 3.22 (4H, td, *J* = 6.8, 10.9 Hz), 1.92 (6H, s), 1.32 (6H, t, *J* = 7.1 Hz). ^{13}C NMR (100 MHz, $CDCl_3$) δ (ppm): 166.2, 152.2, 151.8 ,147.5, 132.6, 129.9, 128.1 127.7, 123.8, 123.0, 118.0, 104.9, 96.8, 77.4, 77.3, 77.1, 76.8, 66.0, 38.4, 16.7, 14.8. Data in agreement with literature values.[52]

Preparation and characterization of rhodamine derivatives (Rh-benz, Rh-phen, and Rh-pyr)

Rhodamine 6G hydrazide (0.125 g, 0.29 mmol) was dissolved in methanol (15 mL). To this solution, two equivalents (0.58 mmol) of the appropriate aldehyde were added (namely, benzaldehyde, 2-hydroxybenzaldehyde, and pyridine-2-carbaldehyde). The mixture was then refluxed for 6 hours. The solvent was removed under reduced pressure and the resultant solid was filtered and washed with diethyl ether (3 × 20 mL), then dried in a desiccator to afford the desired rhodamine derivatives in 80-90% yields.

Rh-benz. ^{1}H NMR (400 MHz, DMSO) δ (ppm): 8.67 (1H, s), 7.90 (1H, d, *J* = 7.0 Hz), 7.62 - 7.54 (2H, m), 7.39 (2H, m), 7.34 (3H, m), 7.04 (1H, d, *J* = 7.5 Hz), 6.33 (2H, s), 6.17 (2H, s), 5.06 (2H, t, *J* = 5.3 Hz), 3.17 - 3.08 (4H, m), 1.83 (6H, s), 1.20 (6H, t, *J* = 7.0 Hz). ^{13}C NMR (100 MHz, $CDCl_3$) δ (ppm): 165.2, 152.3, 151.3, 147.6, 146.5, 135.2, 133.4, 129.6, 128.7, 128.2, 127.7, 127.5, 123.7, 123.4, 118.0, 106.3, 96.7, 77.4, 77.0, 76.7, 65.8, 38.4, 16.7, 14.8. IR (ATR solid, cm^{-1}) 3440 ν_{N-H} (m), 3024, 2968, 2865 ν_{C-H} (m), 1718 $\nu_{C=O}$ lactam (vs). LR-ESI-MS m/z = 517.0 $[M + H]^+$. Elemental analysis calculated for $C_{33}H_{32}N_4O_2$: C 76.72% H 6.24% N 10.84%; found: C 77.01% H 6.12% N 10.86%.

Rh-phen. ^{1}H NMR (400 MHz, $CDCl_3$) δ (ppm): 10.88 (1H, s), 9.11 (1H, s), 8.01 - 7.99 (1H, m), 7.54 - 7.50 (2H, m), 7.18 - 7.11 (2H, m), 7.07 (1H, dd, *J* = 1.5, 7.6 Hz), 6.85 (1H, d, *J* = 8.2 Hz), 6.77 (1H, dt, *J* = 0.9, 11.3 Hz), 6.43 (2H, s), 6.29 (2H, s), 3.50 (2H, s), 3.21 (4H, q, *J* = 7.1 Hz), 1.88 (6H, s), 1.31 (6H, t, *J* = 7.1 Hz). ^{13}C NMR (100 MHz, $CDCl_3$) δ (ppm): 164.3, 158.6, 152.3, 151.8, 151.2, 147.7, 133.6, 131.4, 131.2, 129.7, 128.6, 127.8, 124.1, 123.3, 118.9, 118.5, 118.1, 117.0, 105.6, 96.8, 66.4, 38.3, 16.6, 14.73. IR (ATR solid, cm^{-1}) 3405 ν_{N-H} (m), 2955 ν_{C-H} (m), 1678 $\nu_{C=O}$ (vs) lactam. LR-ESI-MS m/z = 533.3 $[M + H]^+$. Elemental analysis calculated for $C_{33}H_{32}N_4O_3$: C 74.41% H 6.06% N 10.52%; found: C 73.90% H 6.01% N 10.78%.

Rh-pyr. ^{1}H NMR (400 MHz, $CDCl_3$) δ (ppm): 8.45 (1H, qd, *J* = 1.0, 4.7 Hz), 8.24 (1H, s), 8.05 - 8.03 (1H, m), 8.01 (1H, td, *J* = 1.0, 8.1 Hz), 7.59 (1H, dt, *J* = 1.2, 8.0 Hz), 7.47 (2H, qd, *J* = 2.1, 6.4 Hz), 7.12 (1H, qd, *J* = 2.0, 7.4 Hz), 7.07 - 7.04 (1H, m), 6.41 (2H, s), 6.35 (2H, s), 3.48 (2H, s), 3.21 (4H, dd, *J* = 3.3, 6.8 Hz), 1.87 (6H, s), 1.31 (6H, t, *J* = 7.1 Hz). ^{13}C NMR (100 MHz, $CDCl_3$) δ (ppm): 165.6, 154.5, 152.8, 151.1, 149.0, 147.6, 145.4, 136.1, 133.9, 128.3, 127.7, 127.3, 123.7, 123.6, 120.6, 118.0, 105.8, 97.0, 65.7, 38.3, 16.7, 14.8. IR (ATR solid, cm^{-1}) 3442 ν_{N-H} (m), 3010 ν_{C-H} (w), 2967 ν_{C-H} (m), 1719 $\nu_{C=O}$ (vs) lactam. LR-ESI-MS m/z =

518.3 $[M+H]^+$. Elemental analysis calculated for $C_{32}H_{31}N_5O_2$: C 74.25% H 6.04% N 13.53%; found: C 74.00% H 5.99% N 13.02%.

Author Contributions

Conceptualization: MB, KJW, MHI. Data curation: MHI. Formal Analysis: MB, KJW, MHI. Funding acquisition: MB, KJW. Investigation: MHI, GC, ADGJ, FRF. Methodology: MHI, GC. Project administration: MB. Resources: MB, KJW. Software: MB. Supervision: MB, KJW. Visualization: MHI, MB, KJW. Writing – original draft: MHI. Writing – review & editing: MHI, KJW, MB.

Conflicts of interest

There are no conflicts to declare.

Acknowledgements

MB would like to acknowledge support from the US National Science Foundation (NSF) MRI CHE-1919906, NSF MRI CHE-1726812, and NSF OIA-1632825. KJW would like to acknowledge support from NSF OCE-0963064 and the US Army Corps of Engineers Engineer Research and Development Center (ERDC contract W912HZ-19-2-0044). MB also acknowledges support from the Alabama Water Institute at the University of Alabama.

Notes and references

The crystals structure of **Rh-Benz** has been deposited into the CCDC (2168004) and it can be obtained via https://www.ccdc.cam.ac.uk/ or by contacting The Cambridge Crystallographic Data Centre, 12 Union Road, Cambridge CB2 IEZ, UK; fax +44 1223 336033

1. Q. He, G. I. Vargas-Zuniga, S. H. Kim, S. K. Kim and J. L. Sessler, *Chem. Rev.*, 2019, **119**, 9753-9835.
2. T. Bunchuay, A. Docker, U. Eiamprasert, P. Surawatanawong, A. Brown and P. D. Beer, *Angew. Chem., Int. Ed.*, 2020, **59**, 12007-12012.
3. J. M. Mahoney, G. U. Nawaratna, A. M. Beatty, P. J. Duggan and B. D. Smith, *Inorg. Chem.*, 2004, **43**, 5902-5907.
4. K. P. Carter, A. M. Young and A. E. Palmer, *Chem. Rev.*, 2014, **114**, 4564-4601.
5. S.-K. Kim and J. L. Sessler, *Chem. Soc. Rev.*, 2010, **39**, 3784-3809.
6. W.-S. Cho, P. A. Gale and J. L. Sessler, *Anion receptor chemistry*, RSC Publishing, Cambridge, 2006.
7. M. T. Reetz, C. M. Niemeyer and K. Harms, *Angew. Chem.*, 1991, **103**, 1515-1517.
8. Y. Yeon, S. Leem, C. Wagen, V. M. Lynch, S. K. Kim and J. L. Sessler, *Org. Lett.*, 2016, **18**, 4396-4399.
9. S. K. Kim and J. L. Sessler, *Acc. Chem. Res.*, 2014, **47**, 2525-2536.
10. A. P. de Silva, H. G. N. Gunaratne, C. McVeigh, G. E. M. Maguire, P. R. S. Maxwell and E. O'Hanlon, *Chem. Commun.*, 1996, DOI: 10.1039/CC9960002191, 2191-2192.
11. D. Zhang, G. Gao, L. Guy, V. Robert, J.-P. Dutasta and A. Martinez, *Chem. Commun.*, 2015, **51**, 2679-2682.
12. E. Brunetti, J.-F. Picron, K. Flidrova, G. Bruylants, K. Bartik and I. Jabin, *J. Org. Chem.*, 2014, **79**, 6179-6188.
13. Y. Chen, D.-X. Wang, Z.-T. Huang and M.-X. Wang, *Chem. Commun.*, 2011, **47**, 8112-8114.
14. S. J. M. Koskela, T. M. Fyles and T. D. James, *Chem. Commun.*, 2005, DOI: 10.1039/b415522j, 945-947.
15. P. D. Beer, P. K. Hopkins and J. D. McKinney, *Chem. Commun.*, 1999, DOI: 10.1039/A903440D, 1253-1254.
16. S. G. Galbraith, P. G. Plieger and P. A. Tasker, *Chem. Commun.*, 2002, DOI: 10.1039/B208457K, 2662-2663.
17. Q. He, G. M. Peters, V. M. Lynch and J. L. Sessler, *Angew. Chem., Int. Ed. Engl.*, 2017, **56**, 13396-13400.
18. M. Zakrzewski, D. Załubiniak and P. Piątek, *Dalton Trans.*, 2018, **47**, 323-330.
19. K. Gloe, H. Stephan and M. Grotjahn, *Chem. Eng. Technol.*, 2003, **26**, 1107-1117.
20. C. M. Starks, C. L. Liotta and M. Halpern, *Phase-transfer catalysis: fundamentals, applications, and industrial perspectives*, Chapman & Hall, New York, 1994.
21. L. A. J. Chrisstoffels, F. de Jong, D. N. Reinhoudt, S. Sivelli, L. Gazzola, A. Casnati and R. Ungaro, *J. Am. Chem. Soc.*, 1999, **121**, 10142-10151.
22. A. V. Koulov, J. M. Mahoney and B. D. Smith, *Org. Biomol. Chem.*, 2003, **1**, 27-29.
23. J. M. Mahoney, G. U. Nawaratna, A. M. Beatty, P. J. Duggan and B. D. Smith, *Inorg. Chem.*, 2004, **43**, 5902-5907.
24. B. A. Moyer and S. R. P., *Fundamentals and Applications of Anion Separations*, Springer, New York, 2012.
25. J. Rydberg, M. Cox, C. Musikas and G. R. Choppin, *Solvent extraction principles and practice*, CRC Press, 2004.
26. H. Stephan, K. Gloe, W. Kraus, H. Spies, B. Johannsen, K. Wichmann, G. Reck, D. K. Chand, P. K. Bharadwa, U. Müller, W. M. Müller and F. Vögtle, in *Fundamentals and Applications of Anion Separations*, eds. B. A. Moyer and R. P. Singh, Springer, Boston, MA, 2004, DOI: 10.1007/978-1-4419-8973-4_10, pp. 151-168.
27. J. L. Sessler, D. E. Gross, W.-S. Cho, V. M. Lynch, F. P. Schmidtchen, G. W. Bates, M. E. Light and P. A. Gale, *J. Am. Chem. Soc.*, 2006, **128**, 12281-12288.
28. V. Boehmer, A. Dalla Cort and L. Mandolini, *J. Org. Chem.*, 2001, **66**, 1900-1902.
29. D. M. Kneeland, K. Ariga, V. M. Lynch, C. Y. Huang and E. V. Anslyn, *J. Am. Chem. Soc.*, 1993, **115**, 10042-10055.
30. L. Wang, W. Du, Z. Hu, K. Uvdal, L. Li and W. Huang, *Angew. Chem., Int. Ed.*, 2019, **58**, 14026-14043.
31. M. Beija, C. A. M. Afonso and J. M. G. Martinho, *Chem. Soc. Rev.*, 2009, **38**, 2410-2433.
32. E. Manandhar, A. D. G. Johnson, W. M. Watson, S. D. Dickerson, G. S. Sahukhal, M. O. Elasri, F. R. Fronczek, P. J. Cragg and K. J. Wallace, *J. Coord. Chem.*, 2021, **74**, 380-401.
33. H. Li, Z. Liu and R. Jia, *Spectrochim. Acta, Part A*, 2021, **247**, 119095.
34. S. G. Stratton, G. H. Taumoefolau, G. E. Purnell, M. Rasooly, W. L. Czaplyski and E. J. Harbron, *Chem. - Eur. J.*, 2017, **23**, 14064-14072.
35. H. W. Gibson, J. W. Jones, L. N. Zakharov, A. L. Rheingold and C. Slebodnick, *Chem. - Eur. J.*, 2011, **17**, 3192-3206.
36. Y. Marcus and G. Hefter, *Chem. Rev.*, 2006, **106**, 4585-4621.

37. E. E. Bruce, H. I. Okur, S. Stegmaier, C. I. Drexler, B. A. Rogers, N. F. A. van der Vegt, S. Roke and P. S. Cremer, *J. Am. Chem. Soc.*, 2020, **142**, 19094-19100.
38. Y. Marcus, *Chem. Rev.*, 2009, **109**, 1346-1370.
39. S. Roelens, A. Vacca and C. Venturi, *Chem. - Eur. J.*, 2009, **15**, 2635-2644.
40. Y. Wang, H.-Q. Chang, W.-N. Wu, X.-L. Zhao, Y. Yang, Z.-Q. Xu, Z.-H. Xu and L. Jia, *Sens. Actuators, B*, 2017, **239**, 60-68.
41. J.-Q. Qu, L.-F. Wang, Y.-Z. Li, G.-C. Sun, Q.-J. Zhu and C.-G. Xia, *Synth. React. Inorg. Met.-Org. Chem.*, 2001, **31**, 1577-1585.
42. S. Goswami, D. Sen, A. K. Das, N. K. Das, K. Aich, H.-K. Fun, C. K. Quah, A. K. Maity and P. Saha, *Sens. Actuators, B*, 2013, **183**, 518-525.
43. S. Goswami, D. Sen, N. K. Das, H.-K. Fun and C. K. Quah, *Chem. Commun.*, 2011, **47**, 9101-9103.
44. Q. Zhang, Q. Lin, L. Wang, L. Mu and X. Huang, *Pol. J. Chem.*, 2000, **74**, 639-648.
45. Y. Shimura and R. Tsuchida, *Bull. Chem. Soc. Jpn.*, 1956, **29**, 311.
46. L. Mitchell, E. J. New and C. S. Mahon, *ACS Appl. Polym. Mater.*, 2021, **3**, 506-530.
47. R. G. Brereton, *Chemometrics for pattern recognition*, Wiley Interscience, Chichester, U.K., 2009.
48. G. M. Sheldrick, *Acta Crystallographica C - Structural Chemistry*, 2015, **71**, 3-8.
49. G. M. Sheldrick, *Acta Crystallographica A - Foundation and Advances*, 2008, **64**, 112-122.
50. L. J. Barbour, *J. Appl. Crystallogr.*, 2020, **53**, 1141-1146.
51. P. Gans, A. Sabatini and A. Vacca, *Talanta*, 1996, **43**, 1739-1753.
52. Y. Xiang, A. Tong, P. Jin and Y. Ju, *Org. Lett.*, 2006, **8**, 2863-2866.